

# Instabilities of a horizontal shear flow with a free surface

By MICHAEL S. LONGUET-HIGGINS

Institute for Nonlinear Science, University of California, San Diego, La Jolla, CA 92093-0402, USA

(Received 4 August 1997 and in revised form 15 December 1997)

The simple shear-flow model of Stern & Adam (1973), in which a layer of uniform vorticity and depth overlies an infinitely deep fluid, is here extended by the addition of an upper fluid layer of uniform thickness and constant velocity. In this way many experimentally observed velocity profiles can be approximated. The normal mode instabilities of such a model can be found analytically, and their properties calculated through the solution of a quartic polynomial equation. The dispersion relation is here determined and illustrated in its dependence on the Froude number and on the ratio  $H_1/H_2$ , where  $H_1$  and  $H_2$  denote the mean depths of the surface layer and the base of the shear layer, respectively. It is found that two branches of instability which are distinct when  $H_1/H_2$  is moderate or small can become merged when  $H_1/H_2 \geq 0.4924$ . Also calculated are the fastest-growing modes, and their wavelengths. The results are applied to some examples of surface flows generated by towed bodies, and to steady spilling breakers.

---

## 1. Introduction

The theory of the stability of surface shear flows has important applications to the study of surface wakes behind ships or towed bodies (Dimas & Triantafyllou 1994); to the stability of the crest of a spilling breaker (Coakley & Duncan 1997); and to wind-drift currents at the sea surface (Stern & Adam 1973). Such currents are usually unstable, and over large horizontal distances may develop into a turbulent mixing layer. But over short distances they may usefully be treated as steady horizontal shear layers; see for example Peregrine (1974). Theoretical interest then focuses on the normal instabilities of such layers, especially those with the largest growth rates, which can give an indication of the horizontal length scales of the observed perturbations.

The presence of a free surface is an additionally interesting feature. For, whereas mixing layers in an unbounded fluid have been well studied (see especially Winant & Browand 1974), those near a free surface are less well understood.

The simplest theoretical model of a surface shearing current was that due to Stern & Adam (1973), who assumed a surface layer of uniform thickness and vorticity overlying a stationary layer of infinite depth. Other models or developments of the same model are due to Kawai (1977), Voronovich, Lobanov & Rybak (1980), Milinazzo & Saffman (1990), Caponi *et al.* (1991), Morland, Saffman & Yuen (1991) and Shrira (1993).

Recently Dimas & Triantafyllou (1994) have computed the linear stability of a shear flow with a continuous velocity profile of the form

$$u = U \operatorname{sech}^2 by \tag{1.1}$$

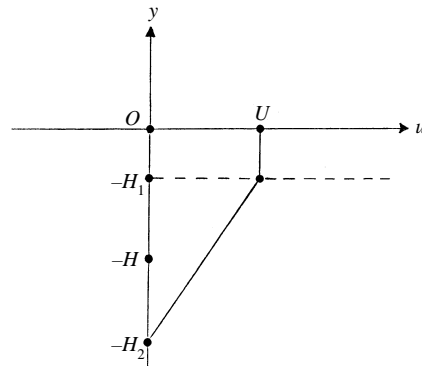


FIGURE 1. Sketch of the velocity profile for the model flow.

(see figure 9 below) and have followed the nonlinear development of a typical sinusoidal instability. It is the linear aspect of the problem which will be considered here. To be precise, Dimas & Triantafyllou find, as in an earlier paper (Triantafyllou & Dimas 1989) that the normal instabilities of the profile (1.1) appear to be of two general kinds: Branch I, which are important at low wavenumbers, and Branch II which are important at high wavenumbers for low Froude numbers, or at low wavenumbers for high Froude numbers. However, their method of calculation is elaborate and their numerical results are consequently incomplete. There seems to be good reason for adopting a much simpler model, representing the observed current profile almost equally well, but amenable to an analytical treatment.

In fact such a model is readily available. It involves simply an extension of the shear-flow model of Stern & Adam (1973) by the addition of a layer of uniform flow immediately below the surface. The model profile depends on three parameters: the surface current  $U$  and the depths  $H_1$  and  $H_2$  of the two upper layers. One particular combination of these parameters fits equation (1.1) reasonably well. Moreover, there is no difficulty in exploring other values of the parameters since the solution to the stability problem is now reduced to determining the roots of a simple quartic polynomial. Not only is this procedure much faster than a purely numerical method, it is also more complete and accurate, and reveals the relation between different branches of the solution in a more transparent way.

In one special case ( $H_1 = 0$ ) the flow reduces to that of Stern & Adam (1973), and in another case ( $H_1 = H_2$ ) it reduces to a thin shear layer at a depth  $H_2$  below the free surface.

The plan of the paper is as follows. Section 2 introduces the model and the basic equations. Section 3 treats especially the boundary conditions, and derives the dispersion relation. This is then discussed, with examples, in §4; see figures 2 to 5. The boundaries of unstable regions are shown in figure 6. In §5 we discuss some special cases. Some comparisons with continuous velocity profiles are given in §6 and in §§7 and 8 we apply the theory to the flow observed in a steady spilling breaker. A general discussion follows in §9.

## 2. Basic equations

Consider a volume of inviscid, incompressible fluid whose velocity  $u$  is directed horizontally in the  $x$ -direction, and depends only on the vertical coordinate  $y$ ; see

figure 1. In particular we take

$$u(y) = \begin{cases} U, & -H_1 < y < 0 \\ \Omega(y + H_2), & -H_2 < y < -H_1 \\ 0, & y < -H_2 \end{cases} \quad (2.1)$$

so that by continuity at  $y = -H_1$

$$U = \Omega(H_2 - H_1). \quad (2.2)$$

It will be convenient to denote the mean depth of the shear layer by

$$H = \frac{1}{2}(H_1 + H_2) \quad (2.3)$$

and to define the Froude number  $F$  by

$$F^2 = U^2/gH. \quad (2.4)$$

Then, if the surface tension  $T$  is neglected, the basic flow depends only on two dimensionless numbers:  $H_1/H$  and  $F$ .

We shall consider sinusoidal perturbations of this flow travelling with phase speed  $c$  to the right. In a frame of reference travelling with the phase speed the two components  $(u, v)$  of the fluid velocity will be given by expressions of the following form. In the upper layer,

$$\left. \begin{aligned} u &= (U - c) + ik(Be^{ky} - Be^{-ky})e^{ikx}, \\ v &= k(Ae^{ky} + Be^{-ky})e^{ikx}. \end{aligned} \right\} \quad (2.5)$$

It is understood that on the right the real part is to be taken. In the intermediate layer,

$$\left. \begin{aligned} u &= \Omega(y + H_2) - c + ik(Ce^{ky} - De^{-ky})e^{ikx}, \\ v &= k(Ce^{ky} + De^{-ky})e^{ikx}. \end{aligned} \right\} \quad (2.6)$$

In the lowest, semi-infinite layer

$$\left. \begin{aligned} u &= -c + ikEe^{ky+ikx}, \\ v &= kEe^{ky+ikx}. \end{aligned} \right\} \quad (2.7)$$

These expressions satisfy the equation of continuity  $\partial u/\partial x + \partial v/\partial y = 0$ . The vorticity is given by

$$\zeta = \frac{\partial v}{\partial x} - \frac{\partial u}{\partial y} = 0, \quad -\Omega, \quad 0 \quad (2.8)$$

in the three regions respectively.

### 3. Boundary conditions

It is assumed that at the free surface the pressure is a constant (zero), and that at the two interfaces both the pressure and the normal velocity are continuous.

The horizontal derivative of the pressure  $p$  is found from the momentum equation

$$\frac{\partial}{\partial x} [p + gy + \frac{1}{2}(u^2 + v^2)] = \zeta v. \quad (3.1)$$

The density is taken to be unity. On linearization, equation (3.1) becomes

$$\frac{\partial}{\partial x} (p + uu') = \zeta v, \quad (3.2)$$

where a prime denotes the perturbation velocity. Using the equation of continuity we then have

$$\frac{\partial p}{\partial x} = u \frac{\partial v}{\partial y} + \zeta v. \quad (3.3)$$

At the free surface  $y = \eta$ , say, the vertical velocity  $v$  is equal to  $u \partial \eta / \partial x$ †. In the linearized theory the boundary condition at the surface can be replaced by the condition that

$$p = (g\eta - T \partial^2 \eta / \partial x^2) \quad (3.4)$$

at the mean surface level  $y = 0$ . Differentiating with respect to  $x$  then gives us

$$u \left( u \frac{\partial v}{\partial y} + \zeta v \right) = gv - T \partial^2 v / \partial x^2 \quad \text{on } y = 0. \quad (3.5)$$

From now on until §7 we neglect surface tension by taking  $T = 0$ . Since  $\zeta$  vanishes in the upper layer we obtain as the upper boundary condition

$$(U - c)^2 \frac{\partial v}{\partial y} = gv \quad \text{on } y = 0. \quad (3.6)$$

Hence from equation (2.5)

$$(U - c)^2 k(A - B) = g(A + B). \quad (3.7)$$

At the interface between the two upper layers, continuity of the normal velocity implies, to first order, the continuity of  $v$ . This and the continuity of  $\partial p / \partial x$  gives us

$$\left. \begin{aligned} Ae^{-kH_1} + Be^{kH_1} &= Ce^{-kH_1} + De^{kH_1}, \\ (U - c)^2(Ae^{-kH_1} - Be^{kH_1}) &= (U - c)^2(Ce^{-kH_1} - De^{kH_1}) \\ &\quad - (U - c)(\Omega/k)(Ce^{-kH_1} + De^{kH_1}). \end{aligned} \right\} \quad (3.8)$$

At the lower interface we find similarly

$$\left. \begin{aligned} Ce^{-kH_2} + De^{kH_2} &= Ee^{-kH_2}, \\ c^2(Ce^{-kH_2} - De^{kH_2}) + c(\Omega/k)(Ce^{-kH_2} + De^{kH_2}) &= c^2 Ee^{-kH_2}. \end{aligned} \right\} \quad (3.9)$$

If we write for short

$$\lambda_1 = e^{-2kH_1}, \quad \lambda_2 = e^{-2kH_2} \quad (3.10)$$

and introduce the notation

$$c_0 = (g/k)^{1/2}, \quad q = U/c_0, \quad Z = \frac{c - U}{c_0} \quad (3.11)$$

and

$$\beta = \frac{\Omega}{kc_0}, \quad (3.12)$$

† This is an approximation, based on the assumption that the rate of growth of the instability is sufficiently small.

then equations (3.7), (3.8) and (3.9) become

$$\left. \begin{aligned} Z^2(A - B) &= A + B, \\ \lambda_1 A + B &= \lambda_1 C + D, \\ Z(\lambda_1 A - B) &= Z(\lambda_1 C - D) + \beta(\lambda_1 C + D), \\ \lambda_2 C + D &= \lambda_2 E, \\ (Z + q)(\lambda_2 C - D) + \beta(\lambda_2 C + D) &= (Z + q)\lambda_2 E. \end{aligned} \right\} \quad (3.13)$$

Eliminating  $E$  between the last two of these equations gives us

$$(Z + q)D - \frac{1}{2}\beta(\lambda_2 C + D) = 0 \quad (3.14)$$

and we are left with four linear equations for  $A, B, C$  and  $D$  with matrix

$$\begin{pmatrix} (Z^2 - 1) & -(Z^2 + 1) & 0 & 0 \\ \lambda_1 & 1 & -\lambda_1 & -1 \\ \lambda_1 Z & -Z & -\lambda_1(Z + \beta) & (Z - \beta) \\ 0 & 0 & -\frac{1}{2}\lambda_2\beta & (Z + q - \frac{1}{2}\beta) \end{pmatrix}. \quad (3.15)$$

The vanishing of the determinant of this matrix gives an equation for  $Z$  and hence the dispersion relation.

#### 4. The dispersion relation

By manipulating rows and columns in (3.15) the vanishing of the determinant becomes equivalent to

$$\begin{vmatrix} (Z^2 - 1) & 2 & 0 & 0 \\ \lambda_1 & -(\lambda_1 + 1) & \lambda_1 & -1 \\ 0 & Z & \lambda_1\alpha & (Z - \alpha) \\ 0 & 0 & \lambda_2\alpha & (Z + q - \alpha) \end{vmatrix} = 0, \quad (4.1)$$

where

$$\alpha = \frac{1}{2}\beta. \quad (4.2)$$

On expansion of the determinant, equation (4.1) reduces to

$$\begin{aligned} &\lambda_1 Z(Z^2 - 1)(Z + q) \\ &+ \lambda_1(\lambda_1 - \lambda_2)\alpha Z(Z^2 + 1) \\ &+ \alpha [\lambda_1 q - (\lambda_1 - \lambda_2)\alpha] [\lambda_1(Z^2 + 1) + (Z^2 - 1)] = 0, \end{aligned} \quad (4.3)$$

a quartic equation for  $Z$ , which may be solved precisely by radicals; see for example Turnbull (1957).

Having obtained  $Z$ , the relation between the wave frequency  $\omega$  (relative to deep water) and the wavenumber  $k$ , can be found from

$$\omega = kc = kc_0(Z + q), \quad (4.4)$$

where  $c_0 = (g/k)^{1/2}$ . For real values of the wavenumber  $k$ , the phase speed is given

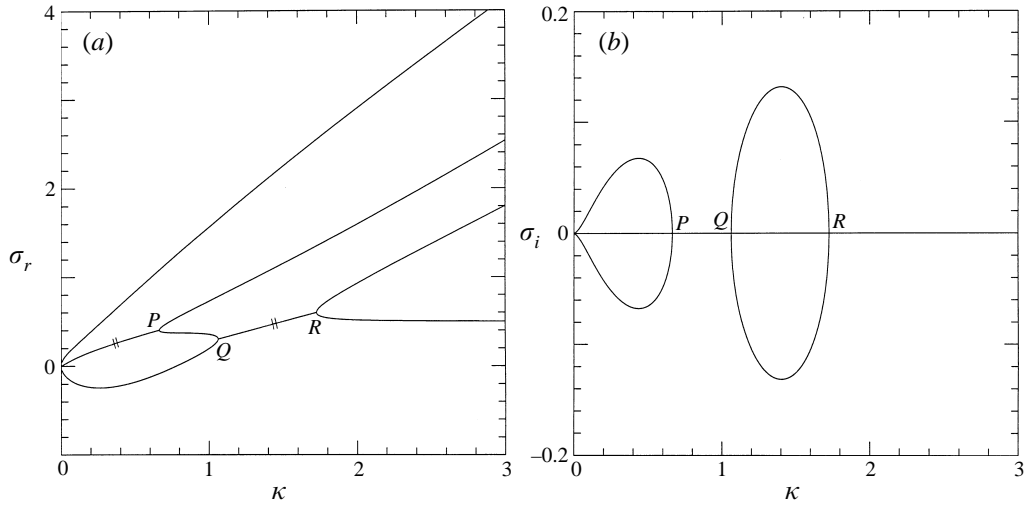


FIGURE 2. The radian frequency  $\sigma_r$  and rate of growth  $\sigma_i$  as functions of  $k$  in dimensionless units, when  $h_1 = 0.5$ ,  $F = 1.5$ .

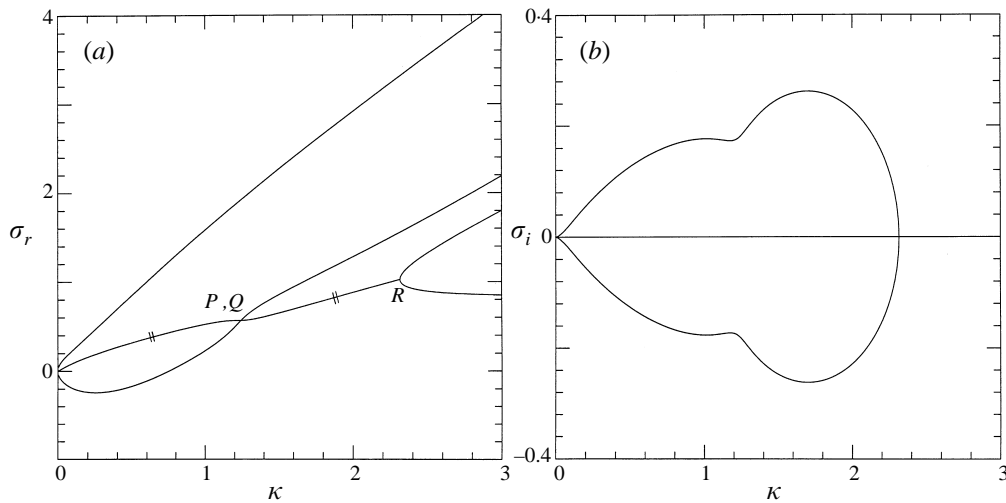


FIGURE 3. As in figure 2, when  $h_1 = 0.7$ ,  $F = 1.5$ .

by  $\omega_r/k$  and the rate of growth by  $\omega_i$ , where  $\omega_r$  and  $\omega_i$  are the real and imaginary parts of  $\omega$ . It is appropriate to plot  $\omega_r$  and  $\omega_i$  as functions of  $k$  for given values of the Froude number  $F = U/(gH)^{1/2}$  and the depth ratio  $H_1/H$ .

For convenience in presentation we introduce the dimensionless wavenumbers and frequency

$$\kappa = kH, \quad (\sigma_r + \sigma_i) = (\omega_r + \omega_i)H/U \quad (4.5)$$

and also the depth ratios

$$h_1 = H_1/H, \quad h_2 = H_2/H \quad (4.6)$$

so that  $h_1 + h_2 = 2$ .

A typical example, when  $h_1 = 0.5$  and  $F = 1.5$ , is shown in figure 2. For large values of  $\kappa$  there are four real roots  $Z$  yielding four separate branches of  $\sigma_r$  (figure 2a).

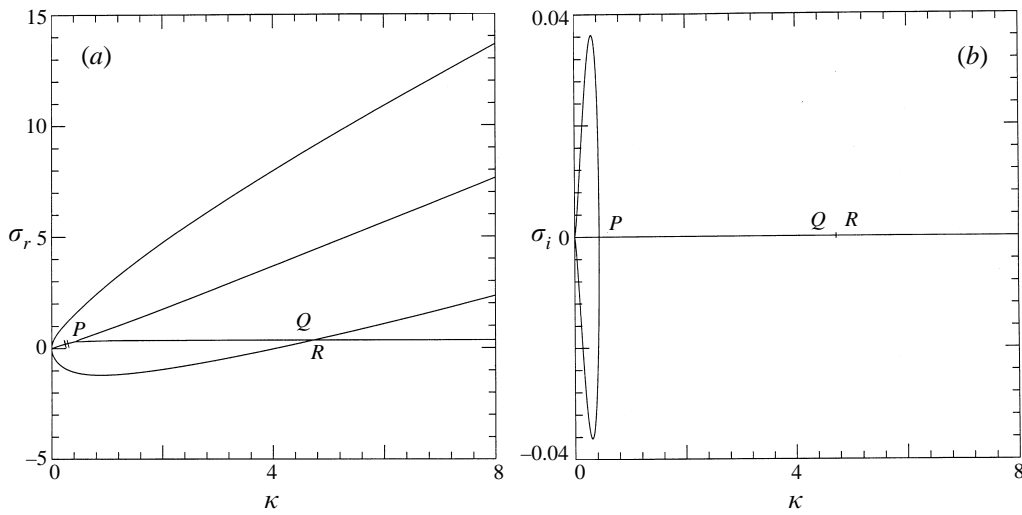


FIGURE 4. As in figure 2, when  $h_1 = 0.3$ ,  $F = 0.5$ .

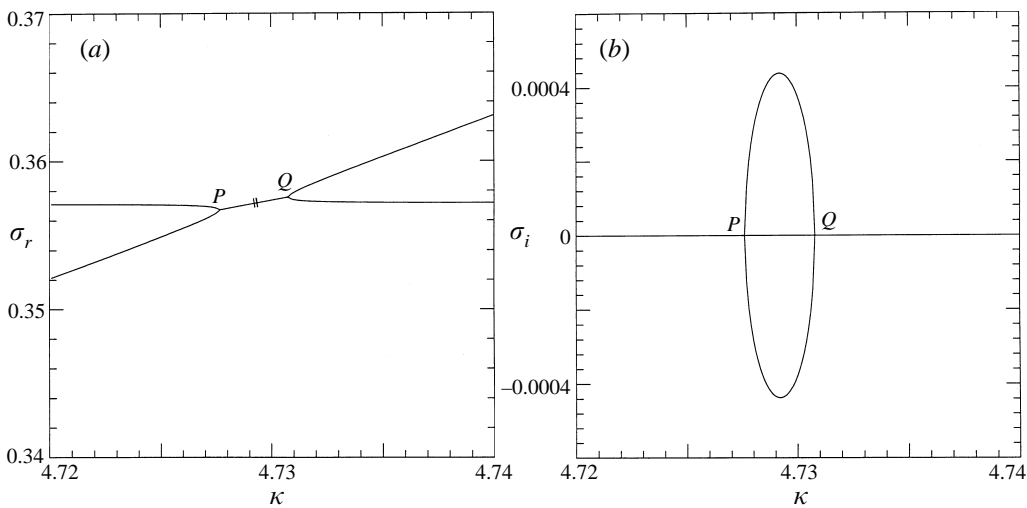


FIGURE 5. Enlargement of figure 4, showing the 'bubble' of instability near  $\kappa = 4.73$ .

However between  $Q$  and  $R$  two of the roots become a conjugate complex pair, and the segment  $QR$  is doubled; this is indicated by a 'parallel' mark. Similarly between 0 and  $P$  another branch is doubled. In each of the intervals  $0P$  and  $QR$ ,  $\sigma_i$  is non-zero (figure 2b).

Figure 3 shows a second example,  $h_1 = 0.7$ ,  $F = 1.5$ . In this case the two points  $P$  and  $Q$  have coalesced into  $PQ$ . The double branch is now continuous through  $PQ$ ; the single branch crosses it with no exchange of stability.

A third example,  $F = 0.5$ ,  $h_1 = 0.3$  is shown in figure 4. This case is similar to figure 2, except that  $Q$  and  $R$  have moved very close together. A blow-up of the region  $QR$  (figure 5) shows that there is a small 'bubble' of instability between  $Q$  and  $R$ .

To obtain a synoptic view, we have plotted in figure 6(a) the wavenumbers  $\kappa$  corresponding to the points  $P, Q, R$ , that is to say the points of marginal stability, for

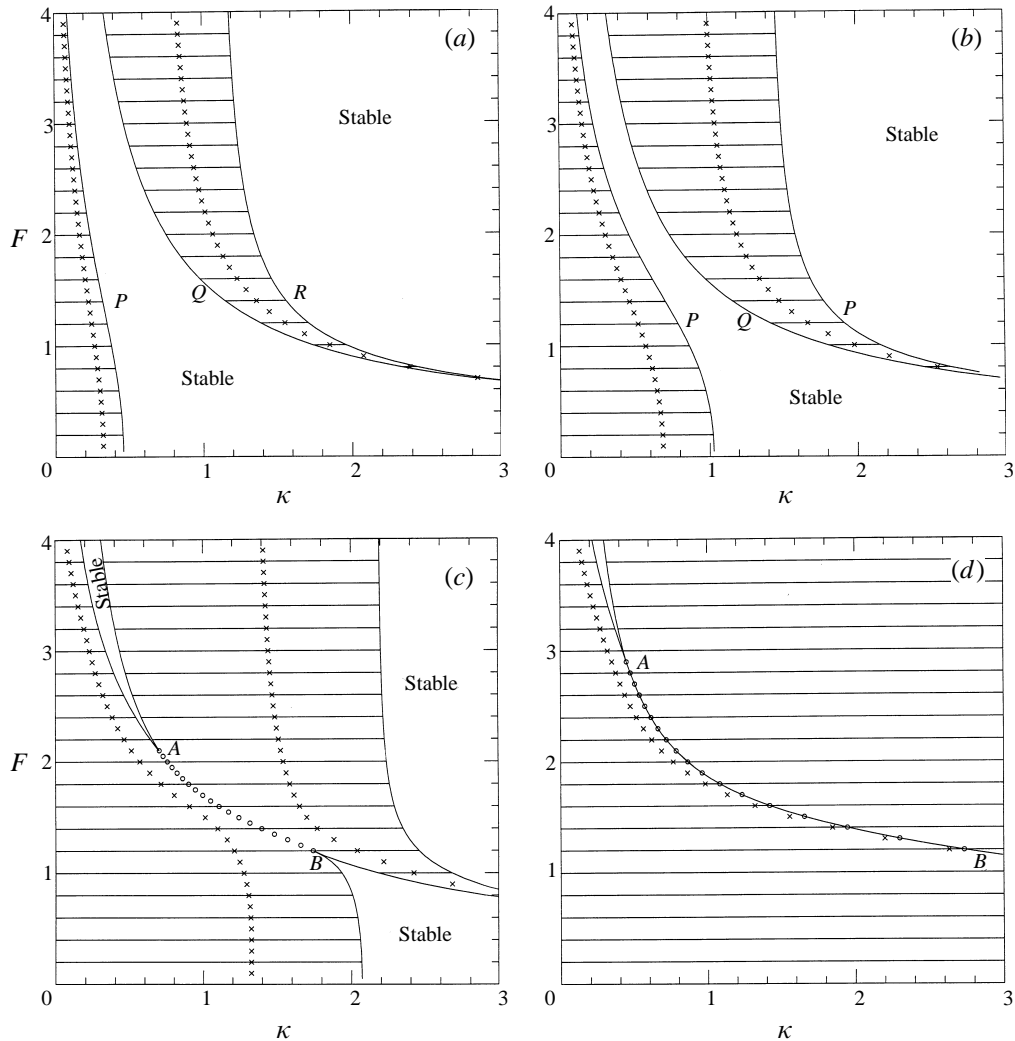
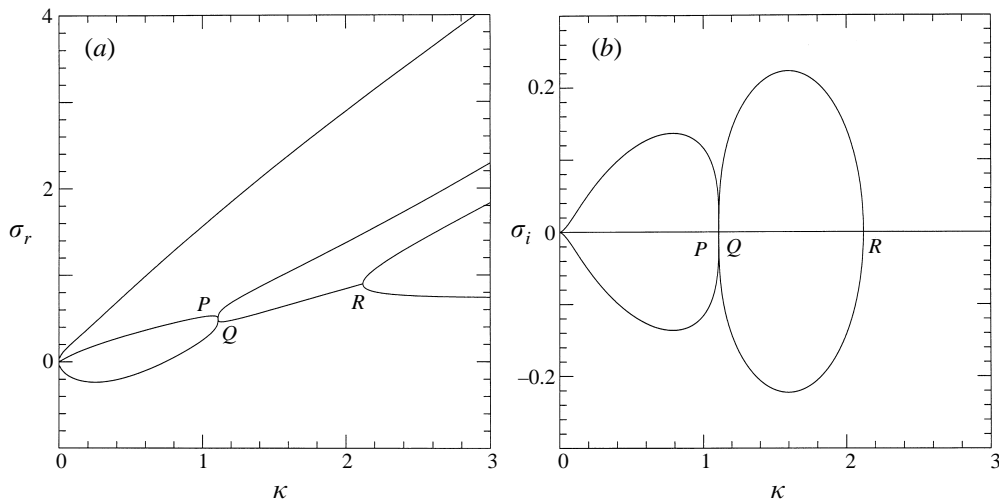
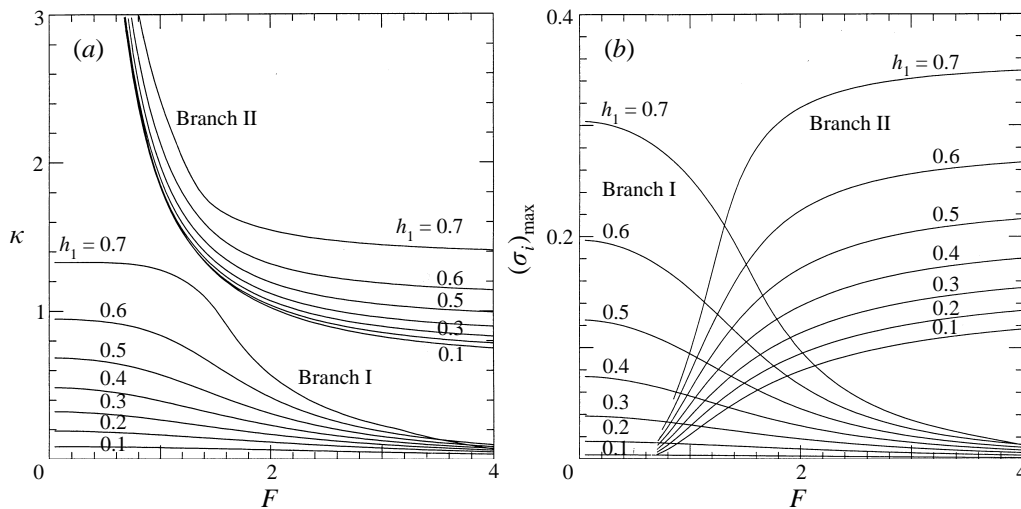


FIGURE 6. Synoptic stability diagrams: full curves, loci of marginal stability; crosses, points of maximum growth rate at constant Froude number  $F$ . (a)  $h_1 = 0.3$ , (b)  $h_1 = 0.5$ , (c)  $h_1 = 0.7$ , (d)  $h_1 = 0.9$ .

values of the Froude number  $F$  (on the vertical axis). It will be seen that there are two distinct areas of stability and two areas of instability. Similarly in Figure 6(b), when  $h_1 = 0.5$ . However in figure 6(c), when  $h_1 = 0.7$ , the two areas of instability have joined in the middle, creating altogether three separate areas of stability. This situation is accentuated in figure 6(d), when  $h_1 = 0.9$ . Now two of the stable areas have moved far to the right, and only a very thin wedge of stability at small wavenumbers remains.

The pinch-off point between figures 6(b) and 6(c), when the two unstable areas just meet, can be determined numerically (see the Appendix) as  $h_1 = 0.6599$  (i.e.  $H_1/H_2 = 0.4924$ ), and  $F = 1.5361$ . The dispersion relation for this particular configuration is shown in figure 7. Three modes coincide at the wavenumber  $\kappa = 1.1091$ .

In each of figures 6(a) to 6(d) the wavenumbers corresponding to maximum rates


 FIGURE 7.  $\sigma_r$  and  $\sigma_i$  as functions of  $\kappa$  for the triple-point mode at  $h_1 = 0.6599$ ,  $F = 1.5361$ .

 FIGURE 8. (a) The maximum growth rate  $\sigma_i$  as a function of  $F$ , at various values of  $h_1$ .  
 (b) The corresponding wavenumber  $k(\sigma_i)$ .

of growth  $(\sigma_i)_{\max}$  have been marked by cross plots. In figures 6(c) and 6(d) the circular plots along the arc  $AB$  correspond to minimum growth rates  $|\sigma_i|$ .

Of special interest are the wavelengths  $(2\pi/k)$  of the fastest-growing modes. The wavenumbers  $\kappa$  are shown in figure 8(a) as functions of  $F$ , for depth ratios  $h_1$  ranging from 0.1 to 0.7. Generally, the wavenumbers increase with increasing  $h_1$ , but decrease with increasing  $F$ , both for Branch I and for Branch II.

The corresponding rates of growth are shown in figure 8(b). Again, the rates of growth generally increase with increasing depth ratio, that is, with decreasing thickness of the vortical layer. The growth rates on Branches I and II are of the same order of magnitude.

### 5. Limiting cases

As  $h_1 \rightarrow 0$  so that the upper layer becomes infinitesimally thin, it is found that the branch point  $P$  in figure 2 moves leftwards towards the origin  $O$ . In the limit, the left-hand curve in figure 6(a) coincides with the vertical axis  $k = 0$ . Setting  $\lambda_1 = 1$  we find that equation (4.3) becomes

$$Z(Z^2 - 1)(Z + q) + (1 - \lambda_2)\alpha Z(Z^2 + 1) + 2\alpha [q + (\lambda_2 - 1)\alpha]Z^2 = 0 \quad (5.1)$$

which has a zero root  $Z$ . Removing this root we are left with a cubic equation which reduces to

$$Z^3 + (m + 2q)Z^2 - (1 + 2\alpha m)Z + m = 0, \quad (5.2)$$

where

$$m = \alpha(1 - \lambda_2) - q. \quad (5.3)$$

This is the same equation as found by Stern & Adam (1973).

Suppose on the other hand that  $h_1$  tends to 1, so that  $(H_2 - H_1)/H \rightarrow 0$  and the shear layer becomes very thin, while remaining at a finite distance  $H$  below the free surface. Then we have

$$\left. \begin{aligned} \lambda_1 - \lambda_2 &\sim 2\kappa(H_2 - H_1), \\ \Omega &= U/(H_2 - H_1) \end{aligned} \right\} \quad (5.4)$$

and hence  $\alpha = \Omega/2kc_0$  becomes large while

$$(\lambda_1 - \lambda_2)\alpha \rightarrow \frac{U}{c_0} = q. \quad (5.5)$$

Then equation (4.3) reduces to

$$\lambda_1(Z^2 + 1) + (Z^2 - 1) = 0 \quad (5.6)$$

so

$$Z^2 = \frac{1 - \lambda_1}{1 + \lambda_1} = \tanh kH_1 \quad (5.7)$$

and

$$\sigma = kU \pm (gk \tanh \kappa H_1)^{1/2}. \quad (5.8)$$

Thus  $\sigma$  has two finite values, which correspond to waves travelling at a speed  $\pm[(g/k) \tanh \kappa H_1]^{1/2}$  relative to the surface current  $U$ . They are similar to gravity waves in the upper layer, propagated as though this shear layer were a rigid boundary.

The remaining roots of equation (4.3) tend to infinity as  $(H_2 - H_1)/H \rightarrow 0$  for finite  $k$ . They represent instabilities of the shear layer itself. As shown in Batchelor (1967, Section 7.1), for example, a shear layer of thickness  $\Delta h$  in an unbounded fluid is unstable to all modes with wavenumber  $k$  of order less than  $(\Delta h)^{-1}$ . In the presence of a free surface, however, the modes can be significantly modified.

Thirdly let us consider the case of low Froude number  $F$ . This is the 'rigid-lid' approximation, when the free surface is assumed to be planar. Then  $q$  and  $\alpha$  are both of order  $F^{-1/2}$ . Equation (4.3) has two roots

$$Z \sim \pm 1, \quad c \sim U \pm c_0 \quad (5.9)$$

which correspond to surface gravity waves travelling in either direction with high speed  $c_0$  relative to the surface current  $U$ . The remaining roots are approximately

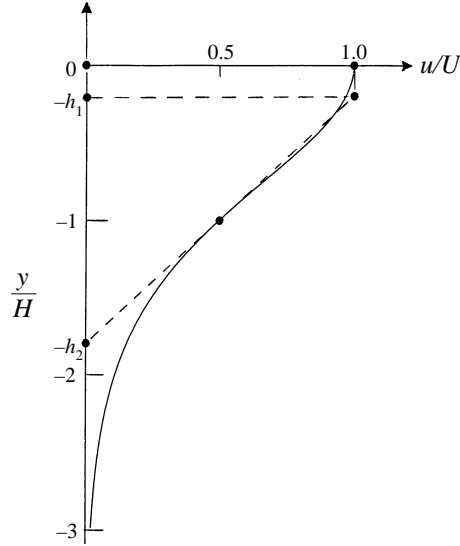


FIGURE 9. The velocity profile given by equation (1.1) (continuous curve), and its approximation by the model profile (2.1).

solutions of the quadratic equation

$$Z(Z + q) + (\lambda_1 - \lambda_2)\alpha Z + \alpha[q - (1 - \lambda_2/\lambda_1)\alpha](\lambda_1 - 1) = 0 \quad (5.10)$$

which is equivalent to

$$(c - U)c + (\lambda_1 - \lambda_2)(\Omega/2k)(c - U) + (\Omega/2k)[U - (1 - \lambda_2/\lambda_1)(\Omega/2k)](\lambda_1 - 1). \quad (5.11)$$

In the further limit  $k \rightarrow 0$  (waves long compared to the depths of the two layers) we have

$$(\lambda_1 - \lambda_2)(\Omega/2k) = (H_2 - H_1)\Omega = U \quad (5.12)$$

and so

$$(c - U)(c + U) = 0 \quad (5.13)$$

or  $c = \pm U$ , to lowest order.

## 6. Comparisons with continuous profiles.

The profile given by equation (1.1), which was adopted by Dimas & Triantafyllou (1994) to fit experimental data of the shear flow in the wake of a hydrofoil is shown in figure 9 (continuous curve). The constant  $b$  in equation (1.1) is chosen so that at the mid-point where  $u = \frac{1}{2}U$  the depth  $-y$  is equal to unity. This implies that

$$e^{by} = \sqrt{2} - 1 \quad (6.1)$$

when  $y = -1$ , and hence

$$b = 0.8814. \quad (6.2)$$

To approximate this profile we may draw a tangent to the curve at the mid-point  $(u, y) = (\frac{1}{2}U, -1)$  and use this to represent a layer of constant shear  $\Omega$ . The velocity

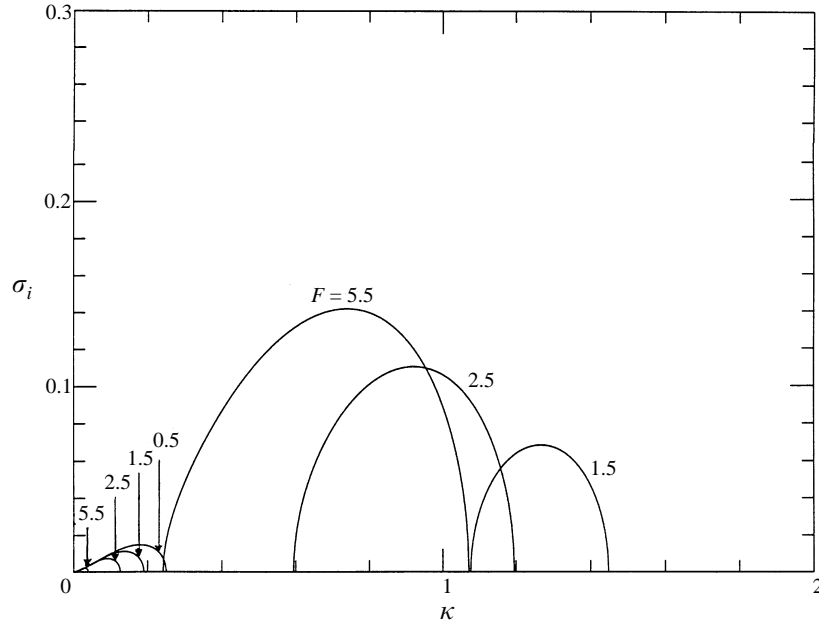


FIGURE 10. The growth rate  $\sigma_i$  as a function of wavenumber for the model profile in figure 9.

gradient at the mid-point is given by

$$\frac{du}{dy} = -2bU \tanh by \operatorname{sech}^2 by = (b/\sqrt{2})U \quad (6.3)$$

and hence

$$-h_1 = 1 - (b\sqrt{2})^{-1} = 0.1977. \quad (6.4)$$

In figure 10 we show the growth rates  $\sigma_i$  calculated as in §5, when  $h_1$  takes the value (6.4), and for Froude numbers  $F = 0.5, 1.5, 2.5$  and  $5.5$ . The two families of curves are qualitatively similar to those calculated numerically for the velocity profile (1.1) by Dimas & Triantafyllou (1994), and shown in their figure 9. Apparently they were unable to present accurate results when  $\sigma_i < 0.01$ . As noted by Morland *et al.* (1991) for the simpler case of the wind-induced drift current, the piecewise linear solution has narrower bands of unstable modes and somewhat higher growth rates.

As a second application consider the velocity profile

$$u = U[1 - \tanh(by^2/b^2)] \quad (6.5)$$

representing the shearing current in the second wave trough behind a steady breaking wave (Duncan & Dimas 1996). Following the same procedure as before we find that the mid-point of the current occurs when

$$e^{by^2/d^2} = \sqrt{3}, \quad y = d \quad (6.6)$$

and hence

$$b = 0.5493. \quad (6.7)$$

Fitting the shear layer by a tangent at the mid-point of the velocity profile we find in a similar way that

$$h_1 = 1 - (3b)^{-1} = 0.3132. \quad (6.8)$$

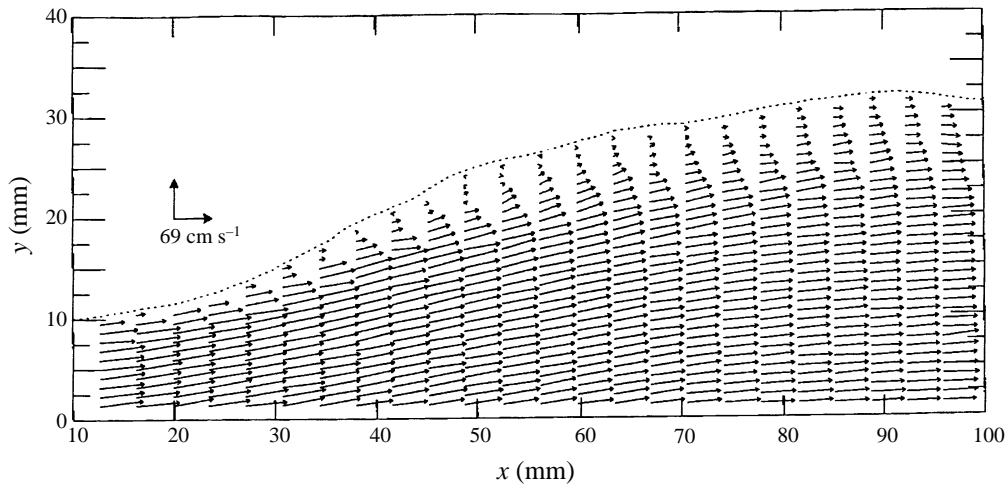


FIGURE 11. (From Coakley & Duncan 1996). Observed fluid velocities relative to a 15 cm hydrofoil towed at a speed of  $69 \text{ cm s}^{-1}$  to the left; average of ten runs.

The Froude number  $F = U/(gH)^{1/2}$  may be determined from their figure 16, in which  $U = 14.8 \text{ cm s}^{-1}$  and  $H = 3.9 \text{ cm}$ , giving  $F = 0.239$ . The dispersion relation, which is similar to figure 4 above, shows there is one maximum growth rate at a dimensionless wavenumber  $\kappa_1 = 0.338$  and a very small bubble of instability at  $\kappa_2 = 18.3$ . These correspond to dimensional wavelengths  $2\pi/k_1 = 72.5 \text{ cm}$  and  $2\pi/k_2 = 1.34 \text{ cm}$  compared with the two wavelengths of 36 cm and 1.4 cm calculated by Duncan and Dimas (1996)†. The present calculations indicate that the rate of growth of the second instability was exceedingly small.

## 7. Application to a steady, spilling breaker

Thirdly we may apply our model to a set of laboratory measurements of the velocity field in a wave induced by a towed hydrofoil (Coakley & Duncan 1996). Figure 11, reproduced from their paper, shows an averaged velocity field from a 15 cm foil towed at a speed of  $69 \text{ cm s}^{-1}$ , in a reference frame travelling with the foil. This indicates that the fluid at the surface has a low velocity compared to the flow beneath. By fitting selected profiles at five equally spaced profiles, as in table 1, we can deduce the parameters  $h_1$  and  $F$  for each profile, as shown in the table. Then from figure 8 above we find the wavenumbers  $\kappa_1$  and  $\kappa_2$ , and the corresponding wavelengths  $L_1$  and  $L_2$ .

A complete comparison with the observed surface profile in figure 11 would have to take account of energy fluxes, including the nonlinear interaction of the waves with the mean flow. At present we simply note that the longer wavelengths  $L_1$  range from 11 to 22 cm, which is comparable to that of the more prominent fluctuations in the observed surface elevation. The shorter wavelengths  $L_2$  lie between 1.6 and 4.0 cm. These are subject to capillarity, which can be taken into account as in §7 below. Additional data, including an instantaneous time sequence of the free surface, would enable the comparison to be pursued further.

† It may be noted that the authors adopt a different definition of  $F$  from that given in §4 above or in Triantafyllou & Dimas (1989).

---

$x$ (mm)	$H_1$ (cm)	$H_2$ (cm)	$U$ (cm s <sup>-1</sup> )	$H$ (cm)	$h_1$	$F$	$\kappa_1$	$L_1$ (cm)	$\kappa_2$	$L_2$ (cm)
20	0.20	0.42	66	0.31	0.64	3.8	0.13	15	1.24	1.6 (1.6)
38	0.25	0.79	58	0.52	0.48	2.6	0.29	11	1.07	3.1 (3.0)
56	0.27	0.85	49	0.56	0.48	2.1	0.27	13	1.16	3.0 (2.9)
74	0.27	1.17	45	0.72	0.37	1.7	0.24	19	1.21	3.8 (3.5)
92	0.27	1.32	45	0.79	0.34	1.6	0.23	22	1.25	4.0 (3.8)

---

TABLE 1. Fitted parameters for the current profiles in figure 11, and the predicted dominant wavelengths

---

### 8. The inclusion of capillarity

The foregoing analysis can easily be modified to include the effect of capillarity. For, it will be seen that the solution of the dispersion relation (4.3) is formally unaltered, for any given wavenumber  $k$ , if only the gravity-wave velocity  $c_0 = (g/k)^{1/2}$  is replaced by the full capillary-gravity velocity  $c_0 = (g/k + Tk)^{1/2}$ . In other words  $g$  has only to be replaced by

$$g' = g + Tk^2. \quad (8.1)$$

Equivalently the Froude number  $F = U/(gH)^{1/2}$  is replaced by  $U/(g'H)^{1/2}$ . The corresponding dispersion relations, and the synoptic diagrams, can be constructed as in figures 2–7, but these will not be shown here. Each depends on the new dimensionless parameter  $T/gH^2$ , which in the present paper has been set to zero. One example of a dispersion relation in which this parameter is not zero, but on the other hand  $h_1$  is zero, is shown in figure 3 of Longuet-Higgins (1994).

Proceeding in this way we have recalculated the wavenumbers and wavelengths shown in table 1. The changes to  $k_1$  and  $L_1$  are negligible. The modified values of  $L_2$  are shown in parentheses.

### 9. Discussion and conclusions

Extending the single-shear-layer model of Stern & Adam (1973) by the addition of an extra surface layer, we have been able to reproduce the stability properties of typical current profiles in the wake of hydrofoils or behind breaking waves, and to simplify their discussion. The previous classification of unstable normal modes into ‘Branch I’ and ‘Branch II’ has been confirmed, but with the restriction that over some ranges of Froude number and depth ratio the two branches are found to merge. A reasonable agreement has been found with the calculations in Duncan & Dimas (1996), and also with the observations by Coakley & Duncan (1997).

It is clear that a simplified model such as that used here can have several advantages over an elaborate numerical scheme. The calculations can be carried out much faster and with greater completeness and accuracy, so that a synoptic view of the solutions can quickly be achieved. At the same time, the slight loss in precision resulting from the initial fitting of the model to the observed current profile is probably unimportant for most purposes.

We have discussed here only the initial development of the instabilities, using linear theory, it being generally assumed that the subsequent flows will be dominated by the most unstable modes. A discussion of the nonlinear stages of development is outside

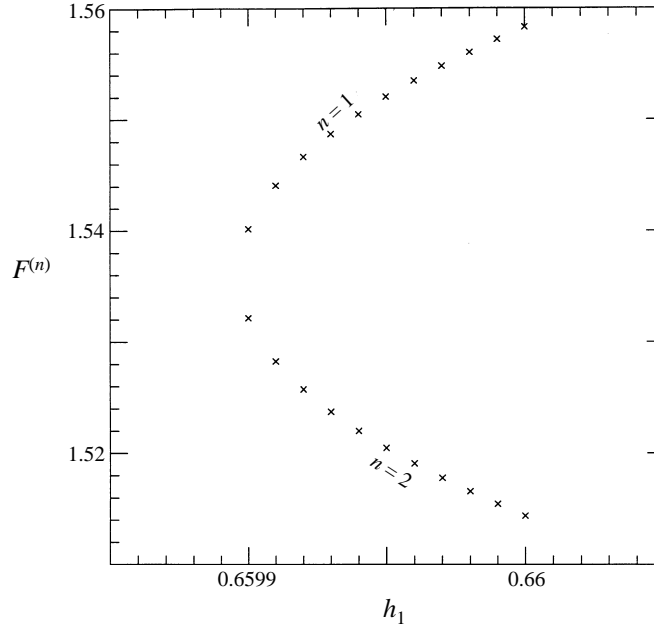


FIGURE 12. Plot of  $F^{(1)}$  and  $F^{(2)}$  as functions of  $h_1$ , close to the critical point.

the scope of this paper, though a nonlinear theory might well be based on the present simplified model.

In this paper we have considered only two-dimensional instabilities. The three-dimensional instabilities of a surface shear layer are likely to be of considerable interest under typical oceanic conditions. Such instabilities could well be investigated by means of a similar simplified approach.

I am indebted to Professor J. H. Duncan for correspondence and for supplying a preprint of Coakley & Duncan (1997). This work has been supported by the Office of Naval Research under Contract N00014-94-1-0008.

#### Appendix. Determination of the critical values of $h_1$ and $F$

We take advantage of two properties of the limiting case: (a)  $Z$  is real, and (b)  $Z$  is a triple root of the quartic equation (4.3). Thus if the polynomial expansion of (4.3) is

$$f(Z) \equiv Z^4 + a_1 Z^3 + a_2 Z^2 + a_3 Z + a_4 = 0 \quad (\text{A } 1)$$

then we have also

$$f'(Z) \equiv 4Z^3 + 3a_1 Z^2 + 2a_2 Z + a_3 = 0 \quad (\text{A } 2)$$

and

$$f''(Z) \equiv 12Z^2 + 6a_1 Z + 2a_2 = 0. \quad (\text{A } 3)$$

From (A 3) we have at once

$$Z = -[3a_1 + (9a_1^2 - 24a_2)^{1/2}]/12 \quad (\text{A } 4)$$

and on substituting into (A 1) and (A 2) we find two simultaneous relations:

$$\phi_1(F, h_1, \kappa) = 0, \quad \phi_2(F, h_1, \kappa) = 0. \quad (\text{A } 5)$$

For any given value of  $h_1$  slightly exceeding the critical value, one can solve equations (A 5) for  $F$  and  $\kappa$  by Newton's method of successive approximation. There are two solutions ( $F^{(1)}, \kappa^{(1)}$ ) and ( $F^{(2)}, \kappa^{(2)}$ ), in general. Close to the critical point, ( $F^{(n)}, h_1$ ) lies closely on a parabola; see figure 12. The critical values of  $h_1$  and  $F$  correspond to the vertex of the parabola, and similarly for  $\kappa^{(n)}$  and  $h_1$ .

## REFERENCES

- BATCHELOR, G. K. 1967 *An Introduction to Fluid Dynamics*. Cambridge University Press, 615 pp.
- CAPONI, E. A., YUEN, H. C., MILINAZZO, F. A. & SAFFMAN, P. G. 1991 Water-wave instability induced by a drift layer. *J. Fluid Mech.* **222**, 207–213.
- COAKLEY, D. B. & DUNCAN, J. H. 1997 The flow field in steady breaking waves. *Proc. 21st Symp. on Naval Hydrodynamics, Trondheim, Norway, 24–28 June 1996*, pp. 534–549. Washington, DC, Natl Acad. Press.
- DIMAS, A. A. & TRIANTYFALLOU, G. S. 1994 Nonlinear interaction of shear flow with a free surface. *J. Fluid Mech.* **260**, 211–246.
- DUNCAN, J. H. & DIMAS, A. A. 1996 Ripples generated by steady breaking waves. *J. Fluid Mech.* **329**, 309–339.
- KAWAI, S. 1977 On the generation of wind waves relating to the shear flow in water. A preliminary study. *Sci. Rep. Tohoku Univ. 5, Geophys.* **24**, 1–17.
- LONGUET-HIGGINS, M. S. 1994 Shear instability in spilling breakers. *Proc. R. Soc. Lond. A* **446**, 399–409.
- MILINAZZO, F. A. & SAFFMAN, P. G. 1990 Effect of a surface shear layer on gravity and gravity-capillary waves of permanent form. *J. Fluid Mech.* **216**, 93–101.
- MORLAND, L. C., SAFFMAN, P. G. & YUEN, H. C. 1991 Waves generated by shear layer instabilities. *Proc. R. Soc. Lond. A* **433**, 441–450.
- PEREGRINE, D. H. 1974 Surface shear waves. *J. Hydraul. Div. ASCE* **100**, 1215–1227.
- SHRIRA, V. I. 1993 Surface waves on shear currents: solution of the boundary-layer problem. *J. Fluid Mech.* **252**, 565–584.
- STERN, M. E. & ADAM, Y. A. 1973 Capillary waves generated by a shear current in water. *Mem. Soc. R. Liège* **6**, 179–185.
- TRIANTYFALLOU, G. S. & DIMAS, A. A. 1989 Interaction of two-dimensional separated flows with a free surface at low Froude numbers. *Phys. Fluids A* **1**, 1813–1821.
- TURNBULL, H. W. 1957 *Theory of Equations*, 5th edn. Edinburgh: Oliver and Boyd, 166 pp.
- VORONOVICH, A. G., LOBANOV, E. D. & RYBAK, S. A. 1980 On the stability of gravitational-capillary waves in the presence of a vertically nonuniform current. *Izv. Atmos. Ocean Phys.* **16**, 220–222.
- WINANT, C. D. & BROWAND, F. K. 1974 Vortex pairing: the mechanism of turbulent mixing-layer growth at moderate Reynolds number. *J. Fluid Mech.* **63**, 237–255.